

Analysis of the Triple Pendulum as a Hyperchaotic System

André E Botha¹ and Guoyuan Qi²

- ¹ Department of Physics, University of South Africa, P.O. Box 392, Pretoria 0003, South Africa
(E-mail: bothaae@unisa.ac.za)
- ² F'SATI and Department of Electrical Engineering, Tshwane University of Technology, Private Bag X680, Pretoria 0001, South Africa
(E-mail: qig@tut.ac.za)

Abstract. An analysis is made of the hyperchaotic behaviour of a triple plane pendulum. It is shown that there are only eight physically distinct equilibrium configurations for the pendulum and that the types of eigen solutions obtained, for the Jacobian matrix evaluated at each equilibrium configuration, are independent of the system parameters. A new method for extracting the periodic orbits of the system is also developed. This method makes use of least-squares minimisation and could possibly be applied to other non-linear dynamic systems. As an example of its use, four periodic orbits, two of which are numerically unstable, are found. Time series plots and Poincaré maps are constructed to investigate the periodic to hyperchaotic transition that occurs for each unstable orbit.

Keywords: Triple pendulum; hyperchaos; fixed points; periodic orbits.

1 Introduction

The present work is motivated by recent interest in studying pendulum systems for possible exploitation in various technological applications. There have been a number of experimental and theoretical investigations aimed at understanding the stability of human gait (manner of stepping) through the use of inverted pendulum models [1,2]. Experimental investigations of either simple or coupled electro-mechanically driven pendulums have been undertaken with the view of developing more precise conditions for the onset of chaos in such systems [3,4]. Also, a triple pendulum suspension system has been developed to seismically isolate optical components on the GEO 600 interferometric gravitational wave detector [5]. The latter development has allowed the detector to achieve a seismic noise sensitivity level which is well below the level from thermal noise.

Coupled pendulums with obstacles have been used to model real mechanical systems that exhibit nonlinear phenomena such as resonances, jumps between different system states, various continuous and discontinuous bifurcations, symmetry breaking and crisis bifurcations, pools of attractions, oscillatory-rotational



attractors, etc. [6–9]. In Ref. [9], for example, it has been shown that a triple pendulum model can provide insight into the real, highly-complicated dynamics of a piston connecting-rod crankshaft system.

An experimental triple pendulum has been constructed by Awrejcewicz *et al.* [10]. This pendulum has been analysed numerically and experimentally, and good agreement has been obtained between the mathematical model and the real system. In the present work, higher order effects that pertain to specific experimental systems, like [10], are neglected. For example, we have not included finer details of the frictional forces that act on the joints of the pendulum, or asymmetries in its driving mechanism. One of the motivating factors for neglecting such higher order effects is the correspondence that exists between the equations for a damped simple pendulum, driven by a constant torque, and the well-known phenomenological model of a superconducting Josephson junction [4,11]. It is thought that our somewhat simplified model of the triple pendulum could, with minor modifications, serve as a useful mechanical analogy for a series system of three resistively coupled Josephson junctions.

This paper is organised as follows. In Section 2, the basic model and equations are described. The system is linearised at its equilibria in Section 3. In Section 4 a new method is developed for finding the periodic orbits of the system, based on least-squares minimisation. Four examples of found periodic orbits are discussed, including their time series and Poincaré maps. In two of the examples interesting periodic-hyperchaotic transitions are observed. Section 5 concludes with a discussion of the main advantages and possible disadvantages of the new method.

2 Description of model and equations

The current work is a continuation of our previous work [12], in which a three-dimensional animation of a model triple plane pendulum was created by using the *Visual* module in the *Python* programming language [14]. As shown in Fig. 1, the model consists of a series of absolutely rigid bars which form the three links of the pendulum (shown in red, green and blue). Additional point-like masses are attached to the bottom of each link (shown as yellow cylindrical disks).

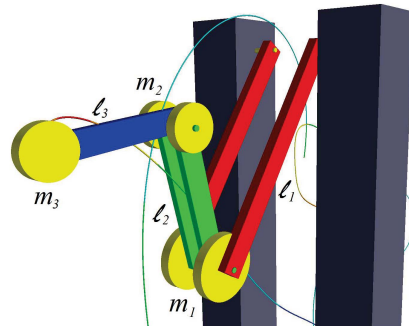


Fig. 1. Visualisation of the triple plane pendulum. The pendulum is made of rigid bars (two of length ℓ_1 , two of length ℓ_2 and one of length ℓ_3) to which point-like masses may be attached (two of mass $\frac{m_1}{2}$, two of mass $\frac{m_2}{2}$ and one of mass m_3). The pendulum is assumed to be under the influence of gravity ($g = 9.81 \text{ ms}^{-2}$) and in vacuum. Also shown is the trajectory followed by the centre of m_3 .

The equations for the pendulum have been derived in a very general form which allows each link in the pendulum to have an arbitrary moment of inertia [8]. In the present work we consider the equations for a pendulum consisting of three point masses, i.e. we neglect the moments of inertia of the three links shown in Fig. 1. The equations for this special case are given in Appendix A of Ref. [12] in the form,

$$\frac{d\mathbf{x}}{dt} = \mathbf{f}(\mathbf{x}, \alpha, t) . \tag{1}$$

In Eq. (1), $\alpha \equiv (m_1, m_2, m_3, \ell_1, \ell_2, \ell_3, c_1, c_2, c_3)$, represents the system parameters, where c_{1-3} model the viscous damping in each joint. The vector $\mathbf{x} \equiv (\theta_1, \theta_2, \theta_3, \dot{\theta}_1, \dot{\theta}_2, \dot{\theta}_3)$, where θ_{1-3} are the angles made between the vertical and each of the three links.

3 Linearisation at the equilibria

The spatial distribution and local dynamical characteristics of the equilibria of a system greatly influence its nonlinear dynamics. Since the un-damped pendulum is conservative, having only time independent constraints, its equilibria are defined by the vanishing of the generalised forces Q_i [13], i.e. by,

$$Q_i = \frac{\partial V}{\partial x_i} = 0 \text{ (for } i = 1, 2, 3) , \tag{2}$$

where $V(x_1, x_2, x_3) = (m_1 + m_2 + m_3)g\ell_1 \cos x_1 + (m_2 + m_3)g\ell_2 \cos x_2 + m_3g\ell_3 \cos x_3$ is the potential energy. The solutions to Eq. (2) produce eight physically distinct equilibria, as shown in Fig. 2.

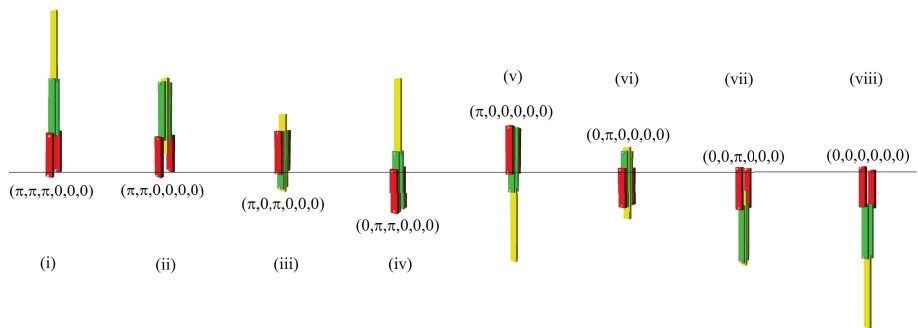


Fig. 2. The eight physically distinct equilibrium configurations of the pendulum. Configurations (i) to (vii) are unstable. Configuration (viii) is stable.

To characterize the linearised dynamics of the system near each equilibrium, we calculate the Jacobian matrix of the system and determine its eigenvalues at the equilibria. The Jacobian matrix, evaluated at any of the equilibria, has

the form

$$\mathbf{J} = \begin{pmatrix} 0 & 0 & 0 & 1 & 0 & 0 \\ 0 & 0 & 0 & 0 & 1 & 0 \\ 0 & 0 & 0 & 0 & 0 & 1 \\ \pm J_1 \pm J_2 & 0 & 0 & 0 & 0 & 0 \\ \pm J_3 \pm J_4 \pm J_5 & 0 & 0 & 0 & 0 & 0 \\ 0 & \pm J_6 \pm J_7 & 0 & 0 & 0 & 0 \end{pmatrix}, \tag{3}$$

where $J_1 = g(m_1 + m_2 + m_3) / (\ell_1 m_1)$, $J_2 = g(m_2 + m_3) / (\ell_1 m_1)$, $J_3 = g(m_1 + m_2 + m_3) / (\ell_2 m_1)$, $J_4 = g(m_1 + m_2)(m_2 + m_3) / (\ell_2 m_1 m_2)$, $J_5 = gm_3 / (\ell_2 m_2)$, $J_6 = g(m_2 + m_3) / (\ell_3 m_2)$ and $J_7 = g(m_2 + m_3) / (\ell_3 m_2)$. To evaluate \mathbf{J} at any particular equilibrium, the signs preceding J_{1-7} in Eq. (3) must be chosen according to the convention given in Table 1.

Equilibrium config.	J_1	J_2	J_3	J_4	J_5	J_6	J_7
(i) $(\pi, \pi, \pi, 0, 0, 0)$	+	-	-	+	-	-	+
(ii) $(\pi, \pi, 0, 0, 0, 0)$	+	-	-	+	-	+	-
(iii) $(\pi, 0, \pi, 0, 0, 0)$	+	-	+	-	+	-	+
(iv) $(\pi, 0, 0, 0, 0, 0)$	+	-	+	-	+	+	-
(v) $(0, \pi, \pi, 0, 0, 0)$	-	+	-	+	-	-	+
(vi) $(0, \pi, 0, 0, 0, 0)$	-	+	-	+	-	+	-
(vii) $(0, 0, \pi, 0, 0, 0)$	-	+	+	-	+	-	+
(viii) $(0, 0, 0, 0, 0, 0)$	-	+	+	-	+	+	-

Table 1. The choice of signs preceding J_{1-7} in Eq. (3) for each of the eight possible equilibrium configurations listed in the left hand column. These combinations of signs should also be used in the definitions of b , c and d in Eq. (4).

The eigenvalues η of the Jacobian matrix were determined by solving the characteristic equation $\det(\mathbf{J} - \eta \mathbf{1}) = 0$, where $\mathbf{1}$ is the 6×6 identity matrix. By choosing all the signs in Eq. (3) to be positive, we found the characteristic equation,

$$0 = a\eta^6 + b\eta^4 + c\eta^2 + d, \tag{4}$$

where $a = 1$, $b = J_1 J_4 J_7 - J_1 J_5 J_6 - J_2 J_3 J_7$, $c = J_1 J_4 - J_2 J_3 - J_1 J_7 - J_4 J_7 + J_5 J_6$ and $d = J_7 - J_1 - J_4$. In the expressions for b , c and d the correct combination of signs, for a particular equilibrium, must once again be chosen from Table 1. For example, for the second equilibrium, row (ii) in Table 1, one obtains $d = (-) J_7 - (+) J_1 - (+) J_4$.

Since Eq. (4) is a cubic polynomial in η^2 , its solutions could be written algebraically [15]. The discriminant of each eigen solution was then used to prove that the type of solution associated with a particular equilibrium configuration is independent of the system parameters. These results are presented in Table 2. To present the complete analysis of the fixed points associated with each equilibrium in Table 2 is beyond the scope of the present article. Briefly, our analysis reveals that (i) to (vii) may be associated with various types of saddle points (depending on the parameter values) and that (viii) will always remain a nonlinear centre.

Table 2. The various types of eigenvalues obtained by solving Eq. (4) at each of the eight possible equilibrium configurations.

Equilibrium config.	Stability	Eigenvalues of \mathbf{J}
(i) $(\pi, \pi, \pi, 0, 0, 0)$	unstable	all real
(ii) $(\pi, \pi, 0, 0, 0, 0)$	unstable	4 real, 2 imaginary
(iii) $(\pi, 0, \pi, 0, 0, 0)$	unstable	4 real, 2 imaginary
(iv) $(\pi, 0, 0, 0, 0, 0)$	unstable	2 real, 4 imaginary
(v) $(0, \pi, \pi, 0, 0, 0)$	unstable	4 real, 2 imaginary
(vi) $(0, \pi, 0, 0, 0, 0)$	unstable	2 real, 4 imaginary
(vii) $(0, 0, \pi, 0, 0, 0)$	unstable	2 real, 4 imaginary
(viii) $(0, 0, 0, 0, 0, 0)$	stable	all imaginary

4 New method for locating periodic orbits

Knowledge of the periodic orbits and their stability is an important aspect of understanding chaotic systems and therefore a great deal of research has already gone into developing more efficient methods for discovering the periodic orbits and periods of non-linear dynamic systems. See, for example, Refs. [16–18], and references therein. In this section we will develop a new method for finding the periodic orbits by making use of the Levenberg-Marquardt algorithm for least-squares estimation of nonlinear parameters [19].

Assume that the system has a periodic orbit with principle period T . As pointed out by Li and Xu [17], it is convenient to use T as one of the optimisation parameters. We therefore re-write Eq. (1) in terms of a dimensionless time parameter τ , by setting $t = T\tau$. This substitution produces the equivalent equation,

$$\frac{d\mathbf{x}}{d\tau} = T\mathbf{f}(\mathbf{x}, \alpha, T\tau) . \tag{5}$$

Since τ is measured in units of T , Eq. (5) has the advantage that it can be integrated over exactly one period, by letting τ run from zero to one.

In order to search for periodic orbits we define the residual (error vector),

$$\mathbf{R} = (\mathbf{x}(1) - \mathbf{x}(0), \mathbf{x}(1 + \Delta\tau) - \mathbf{x}(\Delta\tau), \dots, \mathbf{x}(1 + n\Delta\tau) - \mathbf{x}(n\Delta\tau)), \tag{6}$$

where $\Delta\tau$ is the integration step size. In Eq. (6), n is an integer which must be chosen large enough to ensure that \mathbf{R} has a greater number of components than the number of quantities which are to be optimised simultaneously. This choice is required by the Levenberg-Marquardt algorithm, which is used to locate the global minimum in \mathbf{R} (note that $\mathbf{R} = \mathbf{0}$ for periodic orbits). In the case of the un-damped pendulum, for example, if all possible quantities are to be optimised simultaneously, i.e. six initial conditions, plus six parameters, plus the period (13 quantities); then one must choose $n \geq 2$. The smallest possible choice for this case is $n = 2$, which produces a residual with $6(n + 1) = 18$ components (see Eq. 6).

The definition of \mathbf{R} requires the system to be integrated from $\tau = 0$ to $\tau = 1 + n\Delta\tau$. In the present work we have used a fourth-order Runge-Kutta integration scheme with $n = 3$ and $\Delta\tau = 1/N$, where $N = 2000$. We have

implemented the method in the *Python* programming language [14]. The module *Scipy.optimize* contains the function *leastsq*, which makes use of a modified Levenberg-Marquardt algorithm [20].

When applied to the triple pendulum, the method produces a surprisingly large number of (numerically) stable and unstable periodic orbits. Many of the found orbits at first appear to be qualitatively similar (when viewed on a screen), but are in fact quantitatively different, when studied numerically. In Fig. 3 we have plotted four examples of different periodic orbits that were found. Figure 3 (a) shows a stable symmetric orbit of period $T = 3.0363595$ s.

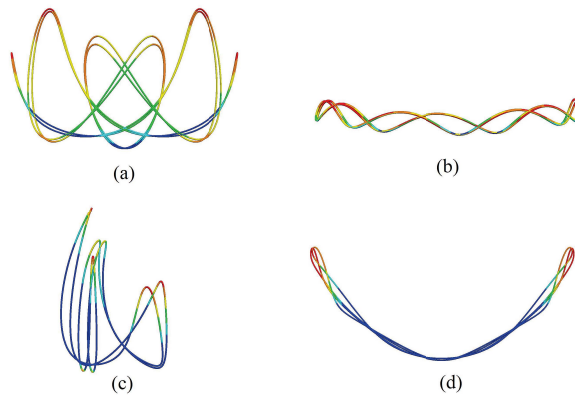


Fig. 3. Four different periodic orbits followed by the centre of m_3 , i.e. here $Y = -\ell_1 \cos x_1 - \ell_2 \cos x_2 - \ell_3 \cos x_3$ is plotted against $X = \ell_1 \sin x_1 + \ell_2 \sin x_2 + \ell_3 \sin x_3$, for the first 10 s. (a) Symmetric and stable. (b) Broken-symmetric and stable. (c) Broken-symmetric and unstable. (d) Symmetric and unstable. The colour of each orbit represents the speed of m_3 in the range zero (red) to 2 ms^{-1} (blue).

One point on the orbit is $(-0.20813379, -0.47019033, 0.80253405, -4.0363589, 4.42470966, 8.3046730)$, with the parameters $m_{1-3} = 0.1 \text{ kg}$, $\ell_1 = 0.15 \text{ m}$ and $\ell_{2-3} = 0.1 \text{ m}$. Figure 3 (b) shows a stable broken-symmetric orbit of period $T = 2.78866884$ s. One point on the orbit is $(-0.22395671, 0.47832902, 0.22100014, -1.47138911, 1.29229544, -0.27559337)$, with the parameters $m_1 = 0.1 \text{ kg}$, $m_2 = 0.2 \text{ kg}$, $m_3 = 0.1 \text{ kg}$, $\ell_1 = 0.15 \text{ m}$, $\ell_2 = 0.2 \text{ m}$ and $\ell_3 = 0.3 \text{ m}$. The Lyapunov exponents for the orbits shown in Figs. 3 (a) and (b) confirm that the orbits are periodic.

Figure 3 (c) shows an unstable broken-symmetric orbit of period $T = 3.23387189$ s. One point on the orbit is $(-0.78539816, 0.79865905, 0.72867705, 0.74762606, 2.56473963, -2.05903234)$, with the parameters $m_1 = 0.35 \text{ kg}$, $m_2 = 0.2 \text{ kg}$, $m_3 = 0.3 \text{ kg}$, $\ell_1 = 0.3 \text{ m}$, $\ell_2 = 0.2 \text{ m}$ and $\ell_3 = 0.25 \text{ m}$. The Lyapunov exponents, sampled every 0.0005 s for 2000 s , confirm that this orbit is hyperchaotic, with $\lambda_1 = 0.90$, $\lambda_2 = 0.19$ and $\lambda_3 = 0.002$. Figure 3 (d) shows an unstable symmetric orbit of period $T = 3.44620156$ s. One point on the orbit is $(1.30564176, 1.87626915, 1.13990186, 0.75140557, 1.65979939, -2.31442362)$, with the parameters $m_1 = 0.35 \text{ kg}$, $m_2 = 0.2 \text{ kg}$, $m_3 = 0.3 \text{ kg}$, $\ell_1 = 0.3 \text{ m}$, $\ell_2 = 0.2 \text{ m}$ and $\ell_3 = 0.25 \text{ m}$. The Lyapunov exponents,

sampled every 0.0005 s for 2000 s, confirm that the orbit is also hyperchaotic, with $\lambda_1 = 2.95$, $\lambda_2 = 1.10$ and $\lambda_3 = 0.004$.

To investigate the rapid transition that occurs from periodic to hyperchaotic the time series and Poincaré maps of each orbit have been studied. Figure 4(a) shows the time series of x_6 for each of the four orbits.

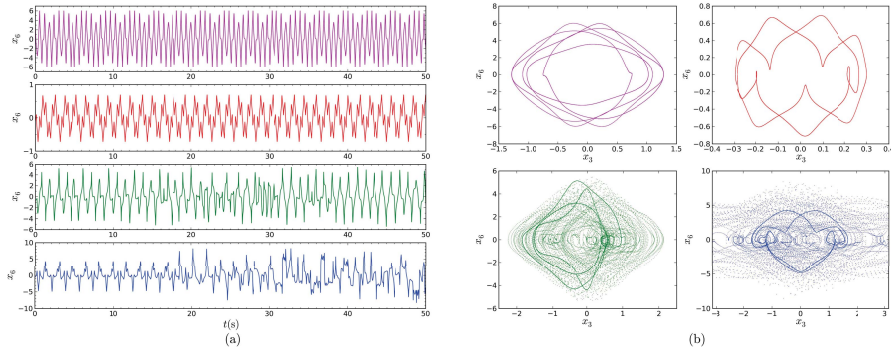


Fig. 4. (a) Time series of x_6 for the orbits discussed in connection with Figs. 3 (a) magenta (top), (b) red, (c) green and (d) blue (bottom). (b) The corresponding Poincaré maps. Parameter values and initial conditions are as for Fig. 3.

The corresponding Poincaré maps, shown in Fig. 4 (b), were constructed by sampling the trajectories every 0.001 s, for 100 s. For this relatively short time interval the periodic parts of the two unstable orbits are still clearly visible within the surrounding (so-called) stochastic layer that is thought to replace the region of destroyed separatrices [21].

5 Discussion and conclusion

The equations for a triple plane pendulum, consisting of three point masses connected by massless links, have been analysed. It was shown that there are only eight physically distinct equilibrium configurations for the pendulum and that the type of eigen solutions obtained for the linearised system at each equilibrium is independent of the system parameter values. A new method for extracting the periodic orbits of the system was also developed. The new method exploits the high-efficiency of the modified Levenberg-Marquardt algorithm. It is simple to implement and does not require the computation of the Jacobian matrix. In addition, the minimisation algorithm may easily be constrained in order to restrict the search to specific regions of the phase space; for example, to a constant energy surface. One possible disadvantage of the method is that it does not discriminate between unstable and stable periodic orbits. However, this aspect of the method may in fact be an important advantage, since it enables the method to be used for studying the coexistence of both regions of stable dynamics and hyperchaos within the phase space.

Acknowledgments

This work is based upon research supported by the National Research Foundation of South Africa (Nos. IFR2011033100063 and IFR2009090800049) and the Eskom–Trust/Tertiary Education Support Programme of South Africa.

References

- 1.K. G. Eltohamy and C. Kuo, *Int. J. of Systems Science* **30**, 505 (1999).
- 2.T. Furuta *et al.*, *Robotics Autonomous Systems* **37**, 81 (2001).
- 3.A. S. de Paula, M. A. Savi, and F. H. I. Pereira-Pinto, *Journal of Sound and Vibration* **294**, 585 (2006).
- 4.M. Gitterman, *The Chaotic Pendulum* (World Scientific, Singapore, 2010).
- 5.M. V. Plissi *et al.*, *Review of Scientific Instruments* **71**, 2539 (2000).
- 6.G. Kudra, Ph.D. thesis, Technical University of Łódź, 2002.
- 7.J. Awrejcewicz and C. H. Lamarque, in *World Scientific Series on Nonlinear Science*, Vol. 45 of *Series A*, ed. L. Chua (World Scientific, Singapore, 2003).
- 8.J. Awrejcewicz, G. Kudra, and C. H. Lamarque, *Int. J. of Bifurcation and Chaos* **14**, 4191 (2004).
- 9.J. Awrejcewicz and G. Kudra, *Nonlinear Analysis* **63**, 909 (2005).
- 10.J. Awrejcewicz *et al.*, *Int. J. of Bifurcation and Chaos* **18**, 2883 (2008).
- 11.S. H. Strogatz, *Nonlinear Dynamics and Chaos* (Addison-Wesley, Reading, 1994).
- 12.A. E. Botha and G. Qi, in *Proceedings of the 56th Annual Conference of the South African Institute of Physics*, edited by I. Basson and A. E. Botha (University of South Africa, Pretoria, 2011), p. 123, ISBN: 978-1-86888-688-3. Available online at www.saip.org.za.
- 13.H. Goldstein, *Classical Mechanics*, 2nd ed. (Addison-Wesley, Reading, 1980), p. 243.
- 14.W. J. Chun, *Core Python Programming* (Prentice Hall, New Jersey, 2007).
- 15.W. Press, S. Teukolsky, W. Vetterling, and B. Flannery, *Numerical Recipes*, 3rd ed. (Cambridge University Press, New York, 2007), p. 228.
- 16.T. Zhou, J. X. Xu, and C. L. Chen, *J. Sound and Vibration* **245**, 239 (2001).
- 17.D. Li and J. Xu, *Engineering with Computers* **20**, 316 (2005).
- 18.D. Li and S. Yang, *Chinese Journal of Applied Mechanics* **28**, 349 (2011).
- 19.D. Marquardt, *SIAM Journal of Applied Mathematics* **11**, 431 (1963).
- 20.H. P. Langtangen, *Python Scripting for Computational Science* (Springer Verlag, Berlin, 2004), p. 161. Also see www.scipy.org.
- 21.G. M. Zaslavsky, *The Physics of Chaos in Hamiltonian Systems*, 2nd ed. (Imperial College Press, Singapore, 2007), p. 2.